February 23, 2008

SCALE LENGTH OF MANTLE HETEROGENEITIES: CONSTRAINTS FROM HELIUM DIFFUSION

S. R. Hart, M. D. Kurz and Z. Wang
Woods Hole Oceanographic Institution
Woods Hole, MA 02543

ABSTRACT

A model of coupled He production/diffusion is used to constrain the question of whether Earth's peridotitic mantle contains ubiquitous mesoscale veins or slabs of other lithologies. The high diffusion rates of helium preclude survival of He isotope heterogeneities on scales smaller than a few tens of meters, especially if they represent long term in-growth of ^{4}He in the mantle. For 1.5 Gy residence times, and a diffusion coefficient of 10^{-10} m^2/sec, 0.5 km slabs or 2 km cylinders will lose >90% of in-grown ^{4}He. However, substantial ^{3}He/^{4}He variations may persist in slabs or be induced in adjacent mantle, depending on initial He, U and Th contents.

We have modeled three cases of ^{3}He/^{4}He equilibration between mantle domains: an ocean crust (OC) slab in depleted upper mantle (DMM) or in enriched mantle (BSE), and a BSE slab in DMM. For a 1 km OC slab in DMM (8 Ra today), the slab today will have ^{3}He/^{4}He of only 3 Ra, and will have influenced the surrounding mantle with ^{4}He for >7 km on either side. The average ^{3}He/^{4}He of this mixed zone will be <7 Ra, even when sampled by melts over a total width of 20-50 km. For the case of a 1 km BSE slab in DMM (8 Ra today), the slab will be 37 Ra today, and will have infected a mantle domain >16 km wide. Even with a 60 km melt sampling width, the average ^{3}He/^{4}He will be >15 Ra.

Slabs may lose their He signature by diffusion, but their presence will be recorded in the surrounding mantle. We have evaluated 3 along-axis N-MORB ridge-crest data sets in this

context (MAR 25.7-26.5°S; EPR 19-23°S; SWIR 16-24°E), with a view to defining scale-lengths of He isotope variability. The average $^3He/^4He$ variability for these 3 areas is very small, and independent of spreading rate: 0.13, 0.19 and 0.21 Ra ($\pm 1\sigma$). Since these ridges range from ultra-slow to very fast-spreading, the variability in size of along-axis magma chambers will lead inevitably to various scales of melt averaging. We conclude that these ridge areas are not sampling mantle that contains enriched veins or recycled oceanic crust slabs of significant size (> tens of meters). It appears difficult to sustain a view of the upper mantle as a ubiquitous mixture of veins and depleted matrix, with MORB always representing an averaging of this mixture.

I. INTRODUCTION

While Earth's mantle is unequivocally heterogeneous, the size, formation and distribution of these geochemical and isotopic heterogeneities remain enigmatic. Following the veined mantle proposals of Hanson (1977) and Wood (1979), a variety of scenarios of small (<1 km) to mesoscale (kms to hundreds of kms) lithologic and geochemical heterogeneities (veins, pods, layers, plums) have been advanced (Zindler et al., 1979, 1984; le Roex et al., 1983; Sleep, 1984; Allegre and Turcotte, 1986). Veins may be visually observed at hand-specimen scale in mantle xenoliths, or at outcrop scale in peridotite massifs. They also may be inferred from chemical or isotopic variability in erupted basalts, especially along the mid-ocean ridge system. However, the issue remains contentious. Do the heterogeneities reflect large scale (tens of km) chemical variability in a lithologically homogeneous (i.e. peridotitic) mantle, or small mesoscale mafic layers or veins embedded in a peridotitic matrix (or a combination of both)? Do the heterogeneities exist as distinct reservoirs, stored in different parts of the earth, or are they

ubiquitously distributed throughout the upper mantle as in the radical Statistical Upper Mantle Assemblage (SUMA) model of Meibom and Anderson (2003) and Meibom et al. (2005)?

We argue, following the proposition by Hanyu and Kaneoka (1998) and Georgen et al. (2003), that the high diffusion rates of helium preclude survival of He isotope heterogeneities on smaller than km scale-lengths, especially if these heterogeneities represent long-term in-growth within the high temperature convecting mantle. We investigate this question with He diffusion/production modeling, and by consideration of He isotope variability along several well-studied spreading ridge systems where only N-MORB is sampled.

II. HE DIFFUSION MODEL WITH PRODUCTION

A large fraction of all the ^{4}He in the earth has been produced by α-decay of U and Th since earth's origin. Thus radiogenic ^{4}He production is an important factor in modeling He behavior in the earth. To illustrate this, we use an infinite slab diffusion model with ^{4}He production; the slab has a half-width in the x-direction of m, symmetric about the y-plane, and is infinite in the y-direction. The He concentration in the slab is $C_1(t,x)$ and the He production is $P_1(t)$. The ^{4}He concentration in the infinite media is $C_2(t,x)$ and the He production is $P_2(t)$.

This infinite slab diffusion model can be described using a one dimensional diffusion equation with a production term, typically written in the following form:

$$\frac{\partial C}{\partial t} = D\frac{\partial^2 C}{\partial x^2} + P(t) \tag{1.1}$$

where C is the concentration of ^{4}He or ^{3}He, D is the effective diffusion coefficient and $P(t)$ is the production term. The following general boundary conditions can be given for this case:

$$C(x,0) = \begin{cases} C_1 & |x| < m \\ C_2 & |x| > m \\ 0 & x = \infty \end{cases} \qquad (1.2)$$

$$P(t) = \begin{cases} P_1(t) & |x| < m \\ P_2(t) & |x| > m \end{cases} \qquad (1.3)$$

The simplest case is for ^{3}He, where there is no production (i.e., $P(t) = 0$) and when $C_2 = 0$ at all times. A typical solution for this one dimensional case can be derived by separation of variables to have the following forms (e.g., Albarède, 1995; equation 8.5.14):

$$C(x,t) = \sum_{n=0}^{\infty} \frac{4C_1}{(2n+1)\pi} e^{-\frac{(2n+1)^2 \pi^2 Dt}{m^2}} \sin \frac{(2n+1)\pi x}{m} \qquad (1.4)$$

If $C_2 = 0$ only when $t = 0$, then the solution will have the following form:

$$C(x,t) = \frac{C_1}{2} \left\{ erf\left(\frac{m-x}{2\sqrt{Dt}} \right) + erf\left(\frac{m+x}{2\sqrt{Dt}} \right) \right\}$$
$$erf(z) = \frac{2}{\sqrt{\pi}} \int_0^z e^{-t^2} dt \qquad (1.5)$$

The general form of $P(t)$ is 0 for ^{3}He, but for radiogenic ^{4}He* is:

$$P(t) = \frac{d(^4He*)}{dt} = 8\lambda_8 {}^{238}U_T e^{\lambda_8(T-t)} + 7\lambda_5 {}^{235}U_T e^{\lambda_5(T-t)} + 6\lambda_2 {}^{232}Th_T e^{\lambda_2(T-t)} = \sum_{i=1}^{3} a_i \lambda_i R_i e^{\lambda_i(T-t)} \qquad (1.6)$$

where T is the age when the system started, t is the elapsed time after age T, $^{238}U_T$, $^{235}U_T$ and $^{232}Th_T$ are present-day concentrations of ^{238}U, ^{235}U and ^{232}Th. λ_8 (0.155125 Gy^{-1}), λ_5 (0.98485 Gy^{-1}) and λ_2 (0.049475 Gy^{-1}) are the decay constants of ^{238}U, ^{235}U and ^{232}Th. a_i is the total number of ^{4}He atoms released from a single U or Th nuclei after decay to Pb. λ_i is the decay constant, R_i is the present concentration of U or Th.

If $C_2 = 0$ at all times and $C_1 = 0$ at $t = 0$, an analytical solution for this case with a production term has the following form (e.g., Albarède, 1995; equation 8.5.20):

$$C(x,t) = \sum_{n=0}^{\infty} \frac{4}{(2n+1)\pi} \sin\frac{(2n+1)\pi x}{m} \int_0^t \sum_{i=1}^{3} a_i \lambda_i R_i e^{\lambda_i(T-u)} e^{\left(-\frac{(2n+1)^2 \pi^2 D(t-u)}{m^2}\right)} du \qquad (1.7)$$

The analytical solutions listed above are for the simple He diffusion and production cases. An analytical solution is not readily available when initial concentration and production terms (i.e., C_1, C_2, P_1 and P_2) are non-zero. We use numerical solutions to solve for more general cases, using commercially available software (COMSOL Multiphysics$^{©}$) equipped with a finite element method. Our infinite slab has a variable half-width (m) with no mass flux across the y-axis center plane (diffusion is symmetrical about the $x = 0$ plane) and no mass flux outside of the box except the concentration is set to be zero at 200 km (so it is effectively a two dimensional infinite slab). The concentration outside the slab is either set to be zero, or left floating depending on the specific case. For the cylinder case, a symmetrical boundary condition is specified on the y-axis. The self-adaptive finite-element mesh was generated automatically by the software, with some manual refinements. A time interval of 0.002 Gy is used, and the relative and absolute tolerance is 10^{-6}. We use one analytic solution for benchmarking (Equation 1.5). This case is for $C_2 = 0$ only when $t = 0$ (e.g. a floating boundary condition), without a production term. A comparison between the numerical and analytical solutions shows that the relative error for the numerical calculation is typically less than 2%, depending on the density of the element mesh and the time interval. The standard temperature and pressure (STP) condition for He is 1 atmosphere and 0°C in all calculations, and the ^{3}He/^{4}He ratio of atmospheric He is 1.399×10^{-6} (Mamyrin et al., 1970; see also Hoffman and Nier, 1993).

For modeling purposes, we have chosen a helium diffusion coefficient of 1×10^{-6} cm^2/sec, which is appropriate as a lower bound for a lherzolitic lithology in the upper mantle. A detailed review of existent helium diffusion measurements, and the likely parameters controlling He transport in the mantle, is given in Appendix I.

For a combined diffusion-production process starting 1.5 Gy ago, for large slab widths (>20 km), the buildup of ^{4}He approaches that of closed system decay of U and Th (see Appendix Fig. A2). With the floating boundary condition, even the thinnest slabs do not approach secular equilibrium between production and diffusion (this occurs only for thin slabs when a zero concentration boundary condition is imposed). Relative to the closed system ^{4}He concentrations, slabs thinner than 1 km continuously lose a large fraction of the radiogenic ^{4}He that is produced (> 80%), indicative of the rapid time constant for slab equilibration with surrounding mantle.

Fig. 1 shows a comparison of ^{4}He retention in a slab and cylinder for several boundary conditions and for both diffusion-only, and diffusion-plus-production (D+P) cases. A system with D = 1×10^{-6} cm^2/s, starting 1.5 Gy ago, with "bulk earth" U and Th contents is used for illustrative purposes (younger starting times would obviously lead to less He loss). Two diffusion-only models are shown, one with the slab boundary held at ^{4}He = 0, all t (curve A), and one with the ^{4}He at the boundary not constrained (allowed to "float") as a function of time (curve D). Comparable diffusion-plus-production models are curve B (contact = 0, all t), and curve E (contact = f(t)). Curve C is for cylindrical geometry, same boundary condition as E.

Retention is dramatically greater when the contact concentration is floating compared to when it is held at zero (e.g. curve E versus B, or curve D versus A). He retention (at a given slab width) is also higher in the D+P cases than in the no-production cases, simply because not all of the He is present throughout the time interval (e.g. curve E versus D, or curve B versus A). A

contact concentration, Cb, held at zero for all time is not realistic for Earth's mantle, as it implies very fast diffusion in the medium outside the slab; the relatively small differences in the diffusion coefficients for the various mantle minerals (Fig. A1) makes this unlikely, unless one were to invoke an ambient mantle with very high grain-boundary volumes (e.g. high-strain zones?), or other short-circuit pathways (e.g. melt networks). In contrast, the diffusion-only cases (e.g. D) may be quite realistic in the mantle, for example in domains where initial He contents are high and U-Th contents (thus production) are low. Thus, for example, curve E will migrate closer to curve D as the initial He content of the slab is increased to values significantly larger than the 1.5 Gy closed-system production inventory of ^{4}He = 7.75x10^{-6} cc/g (see fig. A2).

The least retention occurs in a diffusion-only, Cb = 0, case (A); while unlikely, we show this here as a bound on minimum slab widths required for high He retention (e.g. slab domains greater than 15-20 km thick can be expected to preserve original He isotope signatures).

The cylinder (C) shows less retention than the comparable slab (E), simply due to 2-D versus 1-D transport. A cylinder needs to be 2-3 times larger than a slab to provide comparable He retention (and a spherical geometry would need to be larger than the cylinder by about another factor of ~ 2).

All of the curves in Fig. 1 were calculated with a He diffusion coefficient D^{He} = 1x10^{-6} cm^2/s; because X scales as D$^{0.5}$ in these models, the curves in Fig. 1 can be easily translated in X for other diffusion coefficients by the relation:

$$X_{new} = X_{fig.3} (D_{new}/1x10^{-6})^{0.5} \tag{1.9}$$

Additionally, for widths < 2 km, curve E of figure 1 can be approximated as:

Fraction Retained = 0.22 x width (in km)   (1.10)

Given the above discussion, the most realistic conditions for Earth's upper mantle should be bounded between curves E and C. Significant He exchange ($> 35\%$) will occur for most domains less than 5 km in size, and greater than 90% exchange will occur for scale lengths less than 0.4-1.5 km. Unless mantle domains are significantly younger than 1.5 Gy, larger than 5-10 km, or stored in cooler regions (temperatures $< 1500°C$), it will be very difficult to preserve initial or evolving He isotope signatures without re-equilibration with the ambient mantle.

III. VARIOUS MANTLE DIFFUSION SCENARIOS

Here we will model diffusive He re-equilibration in several specific pseudo-realistic mantle structures, involving combinations of recycled oceanic crust (OC), depleted MORB mantle (DMM), and primitive bulk silicate earth (BSE). The He, U and Th values we have used are given in Table 1. BSE is assumed to start with initial $^3He/^4He \sim 230$ Ra (Harper and Jacobsen, 1996). This value is intermediate between a solar nebula ratio (~120 Ra, Pepin and Porcelli, 2002), and a solar wind ratio (~318 Ra; Wiens et al., 2004); use of the lower solar nebula value would not alter the arguments given here. With a present day BSE of 20 ppb U and Th/U = 4.0 (McDonough and Sun, 1995), BSE is assumed to evolve to $^3He/^4He \sim 50$ Ra today. Note that this value of 50 Ra is not well constrained, as no high $^3He/^4He$ mantle melts in fact have primitive Nd, Pb, Os or Hf isotope ratios. According to the He partitioning work of Parman et al. (2005), He in BSE could be significantly lower than even the 8 Ra of the upper MORB mantle. DMM is assumed to branch off from BSE at 2.5 Gy, and evolve in a single-stage to 8.0

Ra today; realistically, DMM is being continuously depleted over time (Workman and Hart, 2005; Jackson et al., 2008), but this will not qualitatively alter the present modeling (in fact, the ^{3}He content of all reservoirs is constant with time). An ocean crust "packet" is assumed to be derived from this DMM reservoir at 1.5 Gy, and with the estimated He, U and Th contents (Table 1), will evolve to 0.049 Ra today (if in a closed system).

For inter-model comparison, the cases discussed below all utilize a 1.5 Gy starting time, and a 1 km slab thickness imbedded in an infinite ambient mantle. In selected instances, we also show results for 5 km slabs, and diffusion times of 0.5 Gy. A constant He diffusion coefficient of $1x10^{-6}$ cm^2/s is assumed throughout the modeled volume (U and Th are assumed to be immobile; Van Orman et al., 1998).

CASE A: RECYCLED OCEANIC CRUST IN AN AMBIENT DMM MATRIX

This case refers to 1.5 Gy ocean crust subducted into the upper (DMM) mantle, and rapidly stretched and thinned to a 1 km thickness during convection. ^{3}He, ^{4}He and ^{3}He/^{4}He profiles extending to 10 km on either side of the 1 km slab are shown in Fig. 2. Because the ocean crust starts with low ^{3}He (estimated loss by degassing on the ridge, and during subduction, is 96%; see footnote to Table 1, Appendix II), ^{3}He diffusion is directed into the slab from the ambient DMM mantle at all times (Fig. 2a). At present, this crust is not fully equilibrated for ^{3}He, consistent with curve D in Fig. 3. ^{4}He also starts low in the ocean crust (by 96%), but increases rapidly due to production from U + Th (Fig. 2b), becoming higher than ambient DMM within 100 My. Thereafter, this thin slab of ocean crust is a robust ^{4}He source, infecting the ambient mantle for more than 7 km from the slab. Thus, during most of model time, ^{3}He and ^{4}He are diffusing in opposite directions. Additionally, the growth of ^{4}He in the slab outstrips

diffusion, moving further and further from equilibrium with the ambient mantle. The present day ^{4}He content of the slab is predicted to be about 35% of the "closed-system" value for the slab.

Fig. 2c shows the resulting ^{3}He/^{4}He profile for this case; ^{3}He/^{4}He is continuously decreasing over time, and is lower than the far-field DMM value of 8.0 Ra out to a distance of > 7 km. The value of ~ 3 Ra in the slab itself is far from its closed system value of 0.05 Ra, but as ^{3}He approaches equilibrium, and ^{4}He approaches a steady state between production and diffusion (see Fig. A2), the ^{3}He/^{4}He will approach a steady-state of ~ 2.5 Ra.

We now consider the implications of this modeling for melting of this kind of package during recycling into a ridge crest regime. Clearly, if the size of the melting domain is small (~ 1 km), or if the ocean crust slab has a lower melting temperature than the ambient DMM mantle, the resulting melts will exhibit anomalously low ^{3}He/^{4}He ratios. Numerous authors (Hanson, 1977; Wood, 1979; Zindler et al., 1984; Sleep, 1984; Allegre and Turcotte, 1986; Hirschmann and Stolper, 1996) have proposed that the upper mantle is a mixture of two lithologies – a depleted peridotite and assemblages of enriched mafic veins (of assorted heritage). Yet, in general, the ^{3}He/^{4}He ratios of N-MORB are globally clustered around 8 ± 1 Ra, and on regional scales (100s of km) in selected areas may be even more homogeneous (e.g. the southern EPR, see discussion below). Even along the SWIR (Georgen et al., 2003), where the ^{3}He/^{4}He ratios are on average lower than 8.0 Ra, there is no significant small wave-length variability (< 0.2 Ra); this appears inconsistent with the above modeling, as discussed below.

Melting regimes on ridges are almost certainly larger than km-scale. For example, Kenyon and Turcotte (1987), from fluid dynamical considerations, show that the "eddy diffusivity" in basalt melt (derived from a parameterized Nusselt Number) leads to effective mixing in along-ridge magma chambers of up to 50 km. To evaluate this scenario, we

numerically average the profiles in Fig. 2c to determine the ^{3}He/^{4}He ratios as a function of the scale-length of melt averaging, see Fig. 2d. The enormous impact of the slab itself, and its "infection" of ambient mantle, is clearly seen. Even for 40 km melting domains, the ^{3}He/^{4}He ratio of ~ 6.7 Ra is still distinctly lower than the 8.0 Ra of ambient mantle. To represent a case of shorter residence times for ocean crust slabs in the upper mantle, we show a curve in Fig. 2d for 0.5 Gy; as expected, the "infected" volume of DMM is less, but very substantial effects are still present over a 15 km sampling volume. Thicker slabs will infect a larger ambient mantle volume; curves for a 5 km slab injected at both 0.5 Gy and 1.5 Gy are also shown in Fig. 2d.

The effect of multiple thin slabs has also been modeled (not shown), for comparison with the single slab results. Three 50-meter slabs, separated by 1 km, show a smaller overall ^{4}He signal, as the slab "mass fraction" is obviously smaller; the ^{3}He/^{4}He ratio for the central slab is 6.6 Ra (versus ~ 3 Ra for a single 1 km slab). However, the topology and scale-length of the diffusion process is the same, with clearly observable effects in ^{3}He/^{4}He over distances of 10 km.

We also modeled the case of a recycled oceanic crust slab in an ambient BSE matrix. Here the high He content in the BSE matrix rapidly buffers the OC slab to high ^{3}He/^{4}He ratios, so the anomaly due to the slab is small and diffuse. For details, see Appendix III, and Fig. A3.

CASE B: BSE SLAB IN AN AMBIENT DMM MATRIX

This case refers to a BSE slab injected or stirred into a DMM mantle 1.5 Gy ago, and is intended to model a He-rich slab (not necessarily a primitive mantle domain, *sensu stricto*) embedded in a He-depleted mantle. This might be analogous to streaks or veins of a high-He mantle plume that become entrained into the upper mantle; the He profiles are shown in Fig. 3.

Because of the high initial ^{3}He and ^{4}He contents of the slab, He diffusion is directed out of the slab at all times (Fig. 3a and 3b). Even after 1.5 Gy, however, the slab is not fully equilibrated with the ambient mantle, and the ^{3}He/^{4}He of the slab remains far above ambient for all times (Fig. 3c). There is a broad ^{3}He/^{4}He plateau, some 6 km wide, where the ^{3}He/^{4}He ratio is > 37 Ra, compared to the 50 Ra of closed-system BSE today, and the 8 Ra of closed system DMM today. The profiles show idiosyncratic outward-migrating ^{3}He/^{4}He side-lobe bumps, related to the early high ^{3}He/^{4}He flux out of the slab, now preserved in the low ^{4}He-production domain outside the slab. This is similar to the "ghost He" scenario of Albarede and Kaneoka (2007).

When the ^{3}He/^{4}He profile is sampled over varying scale lengths, Fig. 3d, the impact of the high-He slab on the surrounding ambient mantle is enormous. While the ^{3}He/^{4}He ratio at 10 km from the slab is virtually at ambient (8 Ra, Fig. 3c), the ^{3}He/^{4}He ratio of sampling domains as large as 50 km is still > 20 Ra! Fig. 3d shows sampling curves for both 1 km and 5 km slabs. Even more so than in case of an ocean crust slab in DMM, He-rich slabs can "infect" a massive volume of depleted mantle, and it again becomes difficult to reconcile the very uniform ^{3}He/^{4}He of MORB over large scale lengths with the presence of even occasional veins or slabs of either U-rich material (ocean crust) or He-rich material (BSE).

IV. NATURAL CASE STUDIES

In light of the diffusion modeling, it is useful to consider helium data from mid-ocean ridges, in order to document the actual length scales of mantle variability. Hotspot-ridge interactions define the longest length scales. On the Mid-Atlantic Ridge, the highest ^{3}He/^{4}He values are found in central Iceland (65°N), and decrease to the putative N-MORB value (~ 8 Ra), 550 km to the north (Jan Mayen Fracture Zone, 70°N) and 1450 km to the South (Gibbs

Fracture zone, 52°N). This 2000 km along-axis anomaly is also reflected in bathymetric variations, and reflects mixing of large heterogeneous mantle domains during mantle upwelling, rather than the effects of diffusion. There are also somewhat smaller (350 – 800 km) He anomalies along the southern mid-Atlantic ridge (~ 50°), and along the southern East Pacific Rise (~ 17°S and ~ 27°S). In an effort to understand "typical" N-MORB mantle, we have for the most part not considered ridge domains where mixing with plume material or other very large mantle heterogeneities is implicated.

A detailed statistical analysis of $^3He/^4He$ variations along the South-east Indian Ridge (86°-117°E) defines a helium "segregation" length scale of ~ 150 km (Graham et al., 2001). Interestingly, this He variability along the SEIR is totally decoupled from a remarkable bimodality of Hf isotope ratios, that define a "streaky" mantle with a mean scale length of 40 km (Graham et al., 2006).

First, we will discuss several very small scale-length studies, in order to evaluate He isotope variability on km-scale lengths. Then we examine the He isotope variability of "normal" ridge segments from three ridges with different spreading rates, on the assumption that such normal ridge segments provide insight into the ambient upper mantle away from hotspots.

Case A: The smallest scale-lengths

<u>≤ 1 km.</u> Gregg et al (2000) reported He analyses of two MORB pillars from the 1991 eruption at 9°50' N, EPR. Both pillars are from the axial summit graben, separated by ~ 250 m. He analyses on six glass samples from each pillar yielded average values of 8.42 ± 0.06 Ra and 8.43 ± 0.06 Ra (1σ standard deviation). Individual analyses were quoted with errors of 0.03-0.05, so the observed variability is accounted for by analytical uncertainty.

6x20 km.   Geshie et al (2007) reported He analyses of 6 samples collected by submersible from a single slightly off-axis flow field at 14°S on the EPR (this flow field is not a single eruptive unit, and has been divided morphologically into various cones, lobes and plains by Geshi et al, 2007). The samples covered an area of ~ 6x20 km, and the average He value was 8.85 ± 0.29 Ra ($\pm 1\sigma$). Almost the entire observed $^3He/^4He$ range (8.55 to 9.22 Ra) was found between two samples from the same dive (< 4 km track). An on-axis sample 30 km away gave 8.87 ± 0.04 Ra. The flow-field samples show a small variability in $^{87}Sr/^{86}Sr$ (0.70245 – 0.70269), well correlated with trace element indicators such as La/Sm and Zr/K, indicating a range from N-MORB to E-MORB. However, there is no significant correlation between $^3He/^4He$ and either $^{87}Sr/^{86}Sr$ or other trace element indicators of enrichment, suggesting that the relatively small scale-length (~ 5 km) source heterogeneity, witnessed by Sr isotopes and various trace elements, has been diffusively smoothed in the case of $^3He/^4He$. The $^3He/^4He$ variability of ± 0.29 Ra, representing scale lengths of ~ 5 km, will be shown below to be similar to the along-axis variability of $\pm 0.1 – 0.5$ Ra observed at much larger scale lengths (up to 5000 km).

Case B: The very-slow-spreading SW Indian Ridge

The SW Indian Ridge is one of the slowest spreading ridges, with full spreading rates of 8 - 14 mm/yr. Figure 4 shows the helium isotopic data from submarine glasses from the SWIR. The highest values are found near Bouvet Island, just east of the Bouvet triple junction (Kurz et al., 1998). The highest data density is from the long ridge segment between 16°E and 24°E (Georgen et al., 2003), referred to as the orthogonal super-segment. Basalt glass samples from 21 dredge locations along this 490 km super-segment show limited but systematic along-axis

^{3}He/^{4}He variability, Fig. 4, with an approximately linear variation of ^{3}He/^{4}He, from 7.3 Ra in the east to 6.6 Ra in the west. The variability of data about a best-fit linear trend is only $\pm$ 0.11 Ra ($\pm 1\sigma$), compared to the analytical precision of 0.08 Ra (2σ). A number of data points fall off the trend by more than 3σ, so it is likely that some of the small 50-100 km scale variability is real. However, this variability is minor (< 0.2 Ra) in the context of the ~ factor of ten global scale ^{3}He/^{4}He variability. It is also important to note that all of these He ratios are low compared to the "canonical" value of 8 Ra that characterizes most global N-MORB (Georgen et al., 2003).

This orthogonal super-segment is ultra-slow spreading (14 mm/yr full rate) and has typical slow-spreading morphology. It is characterized by 17 individual magmatic segments, 10-35 km in length and elevated by 500-1000 m at their midpoints (Grindlay et al., 1998; 2000; Dulaney, 2002). This is important because it indicates limited along-axis communication of magmatic systems, and therefore a low probability of large-scale magma mixing.

The diffusion modeling shows that veins or slabs of recycled oceanic crust will generate very low ^{3}He/^{4}He over time (~ 0.05 Ra in 1.5 Gy) and could be a source of low ^{3}He/^{4}He. Such slabs however would rapidly equilibrate with ambient DMM mantle (Fig. 1, Fig. 2c), and after equilibration times of 0.5 – 1.5 Gy may retain a ^{3}He/^{4}He signature of 3 - 4 Ra, Fig. 2d. Additionally, these slabs would "infect" a large volume of ambient mantle, such that derived melts may have ^{3}He/^{4}He ratios up to 7-7.5 Ra, if the sampling scale length is large; Fig. 2d.

However appealing this may appear as an explanation for the along-axis He variations on the SWIR, Fig. 4, the modeling scale-lengths are not consistent with the observations. Modeling predicts scale-lengths of He isotope variability of ~ 50 km; these are small compared to the observed large scale variability of ~ 500 km. Given the magmatic segmentation scale of < 50 km derived from the bathymetry (Dulaney, 2002), there is no plausible way to extend the 50 km

scale diffusion domain sampling size to 500 km by along axis mixing. A similar situation was presented by Graham et al., 2001 for the SE Indian Ridge; $^3He/^4He$ ratios showed limited variability on 50 km scale-lengths but peaks of variability at 150-400 km, superimposed on a very large (4500 km) regional gradient.

The ambient mantle could contain a collection of slabs or veins to produce the large scale regional gradient. Georgen et al. (2003) discussed this conceptual model, with vein abundances decreasing from west to east, or with a constant vein/ambient mantle ratio and a melt fraction that varied from west to east. By *ad hoc* distribution of slabs, and their magmatic sampling volumes (Fig. 2d), one could reconstruct the large-scale profile shown in Fig. 4. However, given the fairly steep He isotope gradients shown in Fig. 2, a stochastic distribution of slabs will not suffice, and we prefer to rule out vein models, based on the "Principle of Least Astonishment".

A simpler and more self-evident model posits that the He isotope variations observed from this segment of the SWIR reflect the $^3He/^4He$ composition of a simple peridotitic mantle source. This mantle source may contain very small isotopic variability (e.g. the 0.3 Ra variation over 40 km seen at Longitude 17.7°E, Fig. 4), consistent with the competing effects of diffusion and ^4He production. The 500 km scale "linear" variation, however, simply reflects the long-term evolution of a large mantle domain with very slightly varying (U+Th)/He ratios. For example, in our DMM model (mantle depleted at 2.5 Gy from bulk silicate earth, $^{238}U/^3He$ ratio of 12,690 evolving to 8.0 Ra today), a $^{238}U/^3He$ ratio of 15,562 would evolve to 6.6 Ra (west end, Fig. 4), and a ratio of 14,060 would evolve to 7.3 Ra today (similar results would be obtained from the more realistic continuous depletion model of Jackson et al., 2008). Thus a difference of only 11% in $^{238}U/^3He$ suffices to generate the variation seen in Fig. 4. Additionally, the possible global scale "low He" DMM region in the southern hemisphere discussed by Georgen et al.

(2003), and also obvious in the data of Graham et al (2001), could simply reflect a small (10-20%) ancient global-scale difference in $^{238}U/^{3}He$. The standard model for generation of DMM invokes continuous depletion of the upper mantle by extraction and sequestration of continental (or oceanic) crust – this process will vary on a global scale depending on the locations of sequestration, and can lead to large scale isotopic heterogeneity, provided the competing effects of convective stirring and mixing are not overwhelming. In any event, smooth large-scale isotopic variations, as shown in Fig. 4, are entirely plausible in this way: *res ipsa loquitur*!

Case C: The slow-spreading southern mid-Atlantic Ridge

Published data from the southern Mid-Atlantic Ridge (MAR) are shown in Fig. 5. Although there are fewer large hotspot provinces in the South Atlantic, (e.g., such as Iceland and the Azores in the North Atlantic), some of the along-axis variability is clearly related to ridge-hotspot interactions. The high $^{3}He/^{4}He$ values, up to 15 Ra, between 48° and 52°S are associated with the Discovery and Shona hotspots which have radiogenic Sr and Pb isotopic signatures, enrichments in incompatible trace elements, and anomalous axial depths. Excluding this area, the southern MAR has remarkably constant helium isotopic compositions; the average $^{3}He/^{4}He$ between 0° and 47°S is 7.83 ± 0.47 Ra (1σ, n = 67). This large section of the MAR includes several geochemically anomalous regions characterized by elevated Sr and Pb isotopes. For example $^{87}Sr/^{86}Sr$ values up to .704 are found near Tristan da Cunha (~ 36°S), and there is a broad southward increase in $^{87}Sr/^{86}Sr$ from ~0.7025 to ~0.7035 between 20° and 35°S. Despite these isotopic variations in Sr and Pb, the helium isotopic compositions are remarkably constant.

The densest along-axis sampling are the 13 dredges reported by Graham et al. (1996), for a 90 km ridge segment between 25.7° and 26.5°S, bounded by the Rio Grande and Moore

fracture zones. The full spreading rate here is 35 mm/year. These on-axis (< 2 km) N-MORBS yielded a mean ^{3}He/^{4}He of 7.57 ± 0.13 Ra (1σ). As shown in figure 5, there is a systematic along-axis He isotope variation, with a minimum in ^{3}He/^{4}He of ~ 7.32 Ra near 26°S. Graham et al. (1996) show that this helium minimum is well-correlated with a shoaling of the ridge, from 3800-4000m near the fracture zones, to 2500 meters. This axial swell is also correlated with a negative mantle Bouguer anomaly (Blackman and Forsyth, 1991). While the He is well-correlated (negatively) with a small (~ 1.5%) variation in ^{206}Pb/^{204}Pb (Graham et al., 1996), the Sr and Nd isotopes, and trace element ratios such as La/Sm, are virtually constant (i.e. within analytical precision) across the whole 90 km segment (Castillo and Batiza, 1989; Graham et al., 1996; Niu and Batiza, 1994). In particular, the low ^{3}He/^{4}He samples have identical Sr and Nd (0.70254 and 0.51310) to the average of all the other samples (0.70254 and 0.51312). In all geochemical and isotopic respects, these basalts are garden-variety N-MORB.

It is difficult to reconcile these characteristics with the presence of any kind of vein component in the mantle sources of this segment. First, the slow-spreading rate (35 mm/year full rate) and ridge overlap at 26.2°S argues against significant along-axis mixing of melts. The scale length of dredge sampling (~ 7 km) and the scale length of melt mixing are probably comparable, thus geochemically distinct veins should transfer their signature to erupted melts. Furthermore, there appears to be a variation in degree of melting, from lower near the fracture zones to higher near the axial swell (Batiza et al., 1988; Niu and Batiza, 1994); conventionally, this would enhance a vein component in melts near the bounding fracture zones. Interestingly, there are two groups of seamounts along the Moore Fracture zone (one ~ 40 km east, and one ~ 20 km west of the ridge axes), that have distinctly more radiogenic Sr, Nd and Pb, and higher ^{3}He/^{4}He (up to 10.9 Ra). If the seamount basalts are veined-mantle products, there is clearly no

vestige of these in the on-axis basalts, where La/Sm and Sr and Nd isotopes are uniform, and the axial swell He anomaly has lower, not higher, ^{3}He/^{4}He.

The observed He and Pb isotope variations and the lack of Sr and Nd isotope variations for the ridge crest samples are simply what would be expected of a peridotitic source with a long-term history of minor parent/daughter variability in the degree of depletion. For example, if this depleted mantle was derived from bulk earth 2.5 Gy ago, differences in Rb/Sr, U/He, U/Pb and Sm/Nd of ~ 13%, 6%, 6% and 2% respectively would lead to the observed spread in Sr, He, Pb, and Nd isotopes. The relationship of the Rb/Sr, U/Pb and Sm/Nd variability is about what is expected from mineral/melt partition coefficients (i.e. Rb/Sr>U/Pb>Sm/Nd). U/He partitioning is not as well constrained; the data of Parman et al (2005) would predict the sense of the observed correlation (low ^{3}He/^{4}He with high ^{206}Pb/^{204}Pb), but would not predict as large a fractionation factor for U/He as for U/Pb (except possibly for harzburgites). For this "all-peridotite" model, we estimate the width of the parent/daughter anomaly to be ~ 20 km (which is about the width of the ^{3}He/^{4}He anomaly at "half-height; see Fig. 5). He diffusion will have relatively little effect on an anomaly of this size, beyond some few kms of "broadening; see Fig. 1 and 2. Note that there is an abrupt jump in ^{3}He/^{4}He, from 7.32 to 7.55 (at 26.03°S) over a horizontal distance of only 1.9 km, and this may seem inconsistent with the He diffusion modeling. Suffice to say that melts that are being erupted in close proximity on-axis may have sampling domains that are large and distinct in the Z-direction (especially with a fractal plumbing system; Hart, 1993).

Case D: The super-fast spreading southern East Pacific Rise

Along-axis helium isotopic variability on the super-fast spreading southern EPR is shown in Fig. 6. The full spreading rates in this area are approximately 150 mm/year, roughly 5-10

times faster than the slow spreading examples discussed above, with important implications for mantle upwelling rates and magmatic processes. Magma chambers have been seismically mapped over large extents of this ridge system, with continuous lengths ranging from tens of km up to 175 km in one case (Detrick et al., 1993; Scheirer et al, 1998). The continuity is typically broken at fracture zone offsets, overlapping spreading centers, propagators, etc. The inference is that along-axis magma mixing may be much more effective than on slow spreading ridges, so that km-scale mantle heterogeneities may be mixed out over distances of 50 km or more (depending on the dynamics of mixing in long thin melt-mush zones).

The long-wavelength axial helium isotopic variations are related to the Easter hotspot (25°-27°S; Poreda et al., 1993) and to the region of anomalous melt production near 17°S (Sinton et al., 1991; Niedermann et al., 1997; Kurz et al., 2005). The relatively high ^{3}He/^{4}He ratios (up to ~ 11.5 Ra) in these two regions are associated with clear peaks in the isotopes of Sr, Nd, and Pb. In the 17°S region, the along-axis helium anomaly is much narrower than the Sr-Nd-Pb anomalies. The ^{3}He/^{4}He peak is between 16° and 18°S (see Fig. 6), while the Sr-Nd-Pb anomalies occur between 16° and 20.7°S, i.e. 220 km versus 500 km (Mahoney et al., 1994; Kurz et al., 2005). This difference was interpreted as relating to the melting of an entrained heterogeneity beneath the ridge, where helium is preferentially extracted from the heterogeneity due to greater silicate/melt incompatibility (Mahoney et al., 1994; Kurz et al., 2005). This model implies a significant difference in He concentration between the two regions, whereas the He concentrations are very uniform throughout the entire 16°-20.7°S region (Kurz et al., 2005).

Diffusive equilibration processes could also explain this difference in length scales between He and Sr, Nd and Pb. The extent of equilibration of a high ^{3}He/^{4}He heterogeneity with

surrounding mantle depends on time scales, helium contents and the size of the heterogeneity. A large heterogeneity would preserve both He and Sr, Nd and Pb anomalies. A small heterogeneity could have the He anomaly diffusively erased, while the Sr, Nd and Pb would be preserved. For example, with an equilibration time of 250 Ma (realistic for the upper mantle), a factor of 20 difference in heterogeneity size could explain the observations (derived by scaling of curve E in Fig. 1). A 20 km thick heterogeneity sampled between 16°-18°S would retain a correlated He-Sr-Nd-Pb anomaly pattern. A 1 km thick heterogeneity sampled between18°-20.7°S would have diffusively equilibrated with respect to helium, while retaining the original Sr, Nd and Pb signature. It is not clear that these dimensions are realistic, or that this model works better than the "preferential extraction" model, but it does illustrate the potential for He diffusion to create apparently long wavelength, and non-intuitive, effects relative to other isotope systems.

The region between 18.9°S - 23°S is also of interest because it defines a long segment (460 km) of the super-fast spreading EPR where all of the basalts are N-MORB, with relatively "normal" helium isotopes; see Fig. 6. Sinton et al. (1991) divided this ridge segment into 7 magmatic segments, based on major and trace element data; in addition to this secondary magmatic segmentation, there is a major mantle compositional discontinuity at the 20.7° overlapping spreading center (OSC), seen most clearly in the isotope geochemistry (Mahoney et al., 1994). For example, the $^{87}Sr/^{86}Sr$ drops sharply from ~ 0.7026 north of the OSC to ~ 0.7024 south of the OSC. The $^{3}He/^{4}He$ variations between 18.9°S - 23°S are relatively small, and largely attributable to analytical precision; see Fig. 6. The mean and standard deviation of 21 samples is 8.26 ± 0.19 Ra, with no hint of a "discontinuity" in $^{3}He/^{4}He$ at the 20.7° OSC. Even the ^{4}He concentrations are remarkably uniform across this region, averaging 14 µcc/g (± 4.2 µcc/g), with no perturbation at the OSC. There is an indication of a mild trend of decreasing $^{3}He/^{4}He$ toward

the south; the sampling density and precision is not high enough to verify such a trend, nor to rule out significant small wavelength anomalies (~ 0.4 Ra on 10-20 km scales). Most importantly, there is no evidence for enriched ocean crust (OC) veins embedded in ambient depleted mantle (DMM), as would be predicted by the modeling shown in Fig. 2d. Nor is there evidence of high He veins (e.g. BSE) embedded in DMM, of the kind modeled in Fig. 3d.

V. SUMMARY

At upper mantle temperatures, helium has a diffusivity some 3 - 7 orders of magnitude faster than the other lithophile isotopes (e.g. Sr, Nd, Pb), and this leads to a variety of constraints on the size and nature of chemical heterogeneities in the mantle. Based on a coupled diffusion-production model, cylindrical heterogeneities in the upper mantle less than 2 km in diameter will lose >90% of ^{4}He production in 1.5 Gy, and will only preserve >80% of ^{4}He if the heterogeneity is > 12 km. While small heterogeneities may effectively lose their He isotope "identity" over time, this effect will be mitigated for cases where ^{4}He production is very large (e.g. recycled oceanic crust with high U+Th contents), or where initial He contents are very large relative to the ambient mantle (e.g. "primary" un-degassed mantle). In these cases, which may be common in natural situations, the heterogeneities may remain identifiable, but more importantly they will infect large volumes of surrounding mantle with unmistakable He signatures. In the case of a 1 km ocean crust slab in the upper mantle, the low ^{3}He/^{4}He slab signal will be unmistakable (< 7 Ra) even when averaged into a melt-sampling domain 20-50 km wide. In the case of a 1 km slab of "primary" mantle (high He content, high ^{3}He/^{4}He) embedded in DMM (with ^{3}He/^{4}He = 8 Ra), the ^{3}He/^{4}He will be > 15 Ra even with a 60 km melt sampling domain.

These modeling predictions are evaluated against three selected spreading ridge situations where only N-MORB has been erupted: the ultra-slow SWIR, slow MAR and super-fast EPR.

The SWIR segment of 490 km length shows small ^{3}He/^{4}He variations ($\pm$ 0.11 Ra, n=21) superimposed on a gradient from 6.6 Ra (western end) to 7.3 Ra (eastern end). The 90 km segment of the southern MAR shows a well-defined negative ^{3}He/^{4}He anomaly about 40 km wide, but the overall variability is still only $\pm$ 0.13 Ra (n=14). The 455 km segment on the EPR again shows only minimal ^{3}He/^{4}He variability ($\pm$ 0.19 Ra, n=21). There is no observed correlation between helium isotope variability and spreading rate. Considering the spreading rate and tectonic segmentation of these case study areas, the scale length of along-axis magma mixing is not large enough to homogenize the He variability expected from embedded vein or slab components. While very small veins or layers (< tens of meters) may be invisible after long-term diffusion and eruptive melt processing, the helium isotopic homogeneity argues against the presence of larger slabs, especially of recycled ocean crust composition. In particular, the SUMA model (Meibom and Anderson, 2003; Meibom et al., 2005) of the upper mantle as a ubiquitous mixture of small to moderate scale (1-100 km) enriched and depleted lithologies, with erupted MORB always representing an averaging of this mixture, appears untenable. Ito and Mahoney (2006) propose a similar conceptual model for a heterogeneous OIB-MORB mantle, involving an early-melting high ^{3}He/^{4}He lithology. Because diffusion will decouple helium from any specific lithologies, this model also appears unsustainable.

Acknowledgments

REFERENCES

Albarède, F., 1995. Introduction to Geochemical Modeling. Cambridge University Press, p 543

Albarède, F., Kaneoka, I., 2007. Ghost primordial He and Ne. Geochimica et Cosmochimica Acta 71, A9.

Allègre, C. J., Turcotte, D. L., 1986. Implications of a two-component marble-cake mantle. Nature 323, 123-127.

Batiza, R., Melson, W. G., O'Hearn, T., 1988. Simple magma supply geometry inferred beneath a segment of the Mid-Atlantic Ridge. Nature 335, 428-431.

Blackman, D. K., Forsyth, D. W., 1991. Isostatic Compensation of Tectonic Features of the Mid-Atlantic Ridge: 25-27°30'S. Journal of Geophysical Research 96, 11,741-11,758.

Castillo, P., Batiza, R., 1989. Strontium, Neodymium and lead isotope constraints on near-ridge seamount production beneath the South Atlantic. Nature 342, 262-265.

Detrick, R. S., Harding, A. J., Kent, G. M., Orcutt, J. S., Mutter, J. C., Buhl, P., 1993. Seismic structure of the southern East Pacific Rise. Science 259, 499-503.

Dulaney, T. 2002. Volcanic morphology of the ultraslow spreading Southwest Indian Ridge (15°-35°E): Implications for crustal construction. University of North Carolina, Wilmington.

Georgen, J. E., Kurz, M. D., Dick, H. J. B., Lin, J., 2003. Low ^{3}He/^{4}He ratios in basalt glasses from the western Southwest Indian Ridge (10°-24°E). Earth and Planetary Science Letters 206, 509-528.

Geshi, N., Umino, S., Kumagai, H., Sinton, J. M., White, S. M., Kisimoto, K., Hilde, T. W., 2007. Discrete plumbing systems and heterogeneous magma sources of a 24 km^3 off-axis lava field on the western flank of East Pacific Rise, 14°S. Earth and Planetary Science Letters 258, 61-72.

Graham, D. W., Blichert-Toft, J., Russo, C. J., Rubin, K. H., Albarède, F., 2006. Cryptic striations in the upper mantle revealed by hafnium isotopes in southeast Indian ridge basalts. Nature 440, 199-202.

Graham, D. W., Castillo, P. R., Lupton, J. E., Batiza, R., 1996. Correlated He and Sr isotope ratios in South Atlantic near-ridge seamounts and implications for mantle dynamics. Earth and Planetary Science Letters 144, 491-503.

Graham, D. W., Lupton, J, Spera, F. J., Christie, D. M., 2001. Upper-mantle dynamics revealed by helium isotope variations along the southeast Indian ridge. Nature 409, 701-703.

Graham, D. W., Jenkins, W. J., Schilling, J.-G., Thompson, G., Kurz, M. D., Humphris, S. E., 1992. Helium isotope geochemistry of mid-ocean ridge basalts from the South Atlantic. Earth and Planetary Science Letters 110, 133-147.

Gregg, T. K. P., Fornari, D. J., Perfit, M. R., Ridley, W. I., Kurz, M. D., 2000. Using submarine lava pillars to record mid-ocean ridge eruption dynamics. Earth and Planetary Science Letters 178, 195-214.

Grindlay, N. R., Madsen, J. A., Rommevaux-Jestin, C., Sclater, J., 1998. A different pattern of ridge segmentation and mantle Bouguer gravity anomalies along the ultraslow spreading Southwest Indian Ridge (15°E to 25°E). Earth and Planetary Science Letters 161, 243-

253.

Grindlay, N., Madsen, F. J., Dulaney, T., Smith, D. 2000. Variations in axial relief and gravity anomalies at the Southwest Indian Ridge 15°-35°E., European Geophysical Society Meeting, Geophysical Research Abstracts.

Hanan, B. B., Graham, D. W., Michael, P. J., 1994. Highly correlated lead, strontium, and helium isotopes in Mid-Atlantic Ridge basalts from a dynamically evolving spread center at 31—34°S. Mineralogical Magazine 58A, 370-371.

Hanson, G. N., 1977. Geochemical evolution of the suboceanic mantle. Journal Geological Society London 134, 235-253.

Hanyu, T., Kaneoka, I., 1998. Open system behavior of helium in case of the HIMU source area. Geophysical Research Letters 25, (5), 687-690.

Harper, C. L., Jr., Jacobsen, S. B., 1996. Noble Gases and Earth's Accretion. Science 273.

Hart, S. R., 1993. Equilibration during mantle melting: a fractal tree model, Proceedings of the National Academy of Science 90, 11914-11918.

Hart, S. R., Zindler, A., 1986. In search of a bulk earth composition, Chemical Geology, 57, 247-267.

Hirschmann, M. M., Stolper, E. M., 1996. A possible role for garnet pyroxenite in the origin of the "garnet signature" in MORB. Contributions to Mineralogy and Petrology 124, 185-208.

Hoffman, J. H., Nier, A. O., 1993. Atmospheric Helium Isotopic Ratio, Geophysical Research Letters 20, 121-123.

Hofmann, A. W., 1988. Chemical differentiation of the Earth: the relationship between mantle, continental crust, and oceanic crust. Earth and Planetary Science Letters 90, 297-314.

Hofmann, A., Hart, S. R., 1978, An assessment of local and regional isotopic equilibrium in the mantle. Earth and Planetary Science Letters 38, 44-62.

Ito, G., Mahoney, J. J., 2006. Melting a high ^{3}He/^{4}He source in a heterogeneous mantle. Geochemistry, Geophysics, Geosystems 7, 10.1029/2005GC001158.

Jackson, M. G., Hart, S. R., Saal, A. E., Shimizu, N., Kurz, M. D., Blusztajn, J. S., Skovgaard, A., 2008. Deep mantle plumes expose the Earth's "missing" Titanium, Tantalum and Niobium, G-Cubed, in press.

Kenyon, P. M., Turcotte, D. L., 1987. Along-strike magma mixing beneath mid-ocean ridges: effects on isotopic ratios. Earth and Planetary Science Letters 84, 393-405.

Kurz, M. D., Moreira, M., Curtice, J., Lott, D. E. I., Mahoney, J. J., Sinton, J. M., 2005. Correlated helium, neon, and melt production on the super-fast spreading East Pacific Rise near 17°S. Earth and Planetary Science Letters 232, 125-142.

Kurz, M. D., le Roex, A. P., Dick, H. J. B., 1998. Isotope geochemistry of the mantle near the Bouvet triple junction. Geochimica Cosmochimica Acta 62, 841-852.

Kurz, M. D., Jenkins, W. J., Hart, S. R., Clague, D., 1983. Helium Isotopic Variations in Volcanic Rocks from Loihi Seamount and the Island of Hawaii. Earth and Planetary Science Letters 66, 388-406.

Kurz, M.D., Jenkins, W. J., 1981. The Distribution of Helium in Oceanic Basalt Glasses. Earth and Planetary Science Letters 53, 41-54.

le Roex, A. P., Dick, J. H. B., Erlank, A. J., Reid, A. M., Frey, F. A., Hart, S. R., 1983. Geochemistry, mineralogy and petrogenesis of lavas erupted along the Southwest Indian

Ridge between the Bovet Triple Junction and 11 degrees east. Journal of Petrology 24, 167-318.

Mahoney, J. J., Natland, J. H., White, W. M., Poreda, R., Bloomer, S. H., Fisher, R. L., 1989. Isotopic and geochemical provinces of the western Indian Ocean spreading centers. J. Geophysical Research 94, 4033-4052.

Mahoney, J. J., Sinton, J. M., Kurz, M. D., Macdougall, J. D., Spencer, K. J., 1994. Isotope and trace element characteristics of a super-fast spreading ridge: East Pacific rise, 13 - 23°S. Earth and Planetary Science Letters 121, 173-193.

Mamyrin, B. A., Anufriev, G. S., Kamenskii, I. L., Tolstikhin, I. N., 1970. Determination of the isotopic composition of atmospheric helium. Geochemistry International 7, 498-505.

McDonough, W. F., Sun, S.-s., 1995. The composition of the Earth. Chemical Geology 120, 223-253.

Meibom, A., Anderson, D. L., 2003. The statistical upper mantle assemblage. Earth and Planetary Science Letters 217, 123-139.

Meibom, A., Sleep, N. H., Zahnle, K., Anderson, D. L., 2005. Models for noble gases in mantle geochemistry: Some observations and alternatives. Geological Society of America, Special Paper 388, 347-363.

Moreira, M., Staudacher, T., Sarda, P., Schilling, J.-G., Allègre, C. J., 1995. A primitive plume neon component in MORB: The Shona ridge-anomaly, South Atlantic (51-52°S). Earth and Planetary Science Letters 133, 367-377.

Moreira, M., Blusztajn, J., Curtice, J., Hart, S. R., Dick, H., Kurz, M., 2003. He and Ne Isotopes in oceanic crust: implications for noble gas recycling in the mantle. Earth and Planetary Science Letters 216, 635-643.

Niedermann, S., Bach, W., Erzinger, J., 1997. Noble gas evidence for a lower mantle component in MORBs from the southern East Pacific Rise: Decoupling of helium and neon isotope systematics. Geochimica et Cosmochimica Acta 61, 2697-2715.

Niu, Y., Batiza, R., 1994. Magmatic processes at a slow spreading ridge segment: 26°S Mid-Atlantic Ridge. Journal of Geophysical Research 99, 19,719-19,740.

Parman, S. W., Kurz, M. D., Hart, S. R., Grove, T. L., 2005. Helium solubility in olivine and its implications for high ^{3}He/^{4}He in ocean island basalts. Nature 437, 1140-1143.

Pepin, R.O., Porcelli, D., 2002. Origin of Noble Gases in the Terrestrial Planets, In: Porcelli, D., Ballentine, C. J., Wieler, R., Eds., Noble gases in geochemistry and cosmochemistry, Reviews in Mineralogy and Geochemistry, Vol. 47, pp. 191-246.

Poreda, R. J., Schilling, J.-G., Craig, H., 1993. Helium isotope ratios in Easter Microplate basalts. Earth and Planetary Science Letters 119, 319-329.

Sarda, P., Staudacher, T., Allegre, C. J., 1988. Neon isotopes in submarine basalts. Earth Planetary Science Letters 91, 73-88.

Sarda, P., Moreira, M., Staudacher, T., Schilling, J-G., Allegre, C. J., 2000. Rare gas systematics on the southernmost Mid-Atlantic Ridge: Constraints on the lower mantle and the Dupal source. J. Geophysical Research 105, 5973-5996.

Scheirer, D. S., Forsyth, D. W., Cormier, M., Madcdonald, K. C., 1998. Shipboard geophysical indications of symmetry and melt production beneath the East Pacific Rise near the MELT experiment. Science 280, 1221-1224.

Schmerr, N., Garnero, E., 2006. Investigation of upper mantle discontinuity structure beneath the central Pacific using SS precursors. Journal of Geophysical Research 111, B08305, doi:10.1029/2005JB004197.

Sinton, J. M., Smaglik, S. M., Mahoney, J. J., Macdonald, K. C., 1991. Magmatic processes at superfast spreading mid-ocean ridges: glass compositional variations along the East Pacific Rise. Journal of Geophysical Research 96, 6133-6136.

Sleep, N. H., 1984. Tapping of magmas from ubiquitous mantle heterogeneities: an alternative to mantle plumes? Journal of Geophysical Research 89, 10,029-41.

Sneeringer, M., Hart, S. R., Shimizu, N.,1984. Strontium and Samarium diffusion in diopside, Geochim. Cosmochim. Acta, 48, 1589-1608.

Staudacher, T., Sarda, P., Richardson, S. H., Allegre, C. J., Sagna, I., Dimitriev, L. V., 1989. Noble gases in basalt glasses from a Mid-Atlantic Ridge topographic high at 14°N: Geodynamic consequences. Earth Planetary Science Letters 96, 119-133.

Stronick, N. A., Niedermann, S., Haase, K. M., 2007. Neon and helium isotopes as tracers of mantle reservoirs and mantle dynamics. Earth and Planetary Science Letters 258, 334-344.

Wiens, R. C., Bochsler, P., Burnett, D. S., Wimmer-Schweingruber, R. F., 2004. Solar and solar-wind isotopic compositions, Earth and Planetary Science Letters 222, 697-712.

Wood, D. A., 1979. A variably veined suboceanic upper mantle-Genetic significance for mid-ocean ridge basalts from geochemical evidence. Geology 7, 499-503.

Workman, R. K., Hart, S. R., 2005. Major and Trace Element Composition of the Depleted MORB Mantle (DMM). Earth and Planetary Science Letters 231, 53-72.

Zindler, A., Hart, S. R., Frey, F. A., Jakobsson, S., 1979. Nd and Sr isotope ratios and REE abundances in Reykjanes peninsula basalts: Evidence for mantle heterogeneity beneath Iceland. Earth and Planetary Science Letters 45, 249-262.

Zindler, A., Staudigel, H., Batiza, R., 1984. Isotope and trace element geochemistry of young Pacific seamounts: implications for the scale of upper mantle heterogeneity. Earth and Planetary Science Letters 70, 175-195.

Figure Captions

Fig. 1. Percent ^{4}He retained in a slab as a function of slab width, comparing different models (all with 1.5 Gy start of model, U and Th restricted to slab, $D^{He} = 1 \times 10^{-6}$ cm^2/s both inside and outside the slab). While cast here as He retention, it can also be thought of as: fraction of He exchange = 1- fraction retention. Curves A and D (dashed lines) are models with diffusion only, no production, initial ^{4}He $= 1 \times 10^{-5}$ cc/g inside the slab, zero outside the slab; in A, the contact is

held at zero concentration for all t; in D, the contact concentration is allowed to float as a f(t). Curves B and E are models with both diffusion and production, initial ^{4}He = 0 throughout, 20 ppb U inside the slab (today); in B, the contact is held at zero concentration for all t; in E, the contact concentration is allowed to float as a f(t), which is the same case as used in Fig. 2. Curve C is for a cylinder of diameter = slab width, with both diffusion and production (20 ppb U), initial ^{4}He = 0, contact concentration floating as f(t).

Fig. 2. Time evolution over 1.5 Gy of (a) ^{3}He, (b) ^{4}He, (c) ^{3}He/^{4}He profiles orthogonal to an infinite 1 km slab of ocean crust (OC) embedded in an infinite medium of DMM (depleted MORB mantle). Model parameters are given in Table 1. Profiles are shown for 1.5 Gy (initial condition), and 1.4, 1.3, 1.0, 0.5 Gy and Today. Panel (d) shows the average ^{3}He/^{4}He ratios of various size sampling boxes, centered on both a 1 km and a 5 km slab, after either 0.5 Gy or 1.5 Gy of coupled He diffusion and production.

Fig. 3. Time evolution over 1.5 Gy of (a) ^{3}He, (b) ^{4}He, (c) ^{3}He/^{4}He profiles orthogonal to an infinite 1 km slab of BSE (bulk silicate earth mantle) embedded in an infinite medium of DMM (depleted MORB mantle). Model parameters are given in Table 1. Profiles are shown for 1.5 Gy (initial condition), and 1.4, 1.3, 1.0, 0.5 Gy and Today. Panel (d) shows the average ^{3}He/^{4}He ratios of various size sampling boxes, centered on both a 1 km and a 5 km slab, after either 0.5 Gy or 1.5 Gy of coupled He diffusion and production.

Fig. 4. ^{3}He/^{4}He variations for basalt glass from the SW Indian Ridge between 0°-70°E (data from Sarda et al., 1988; Mahoney et al., 1989; Kurz et al., 1998; Georgen et al., 2003). Data for the

island of Bouvet is indicated by the circled B. Lower panel is an enlargement showing 21 dredges along the Orthogonal Super-segment between 16°-24°E, from Georgen et al, 2003. Except for three samples from one dredge (19.10°E) that are from sample fusions, all others are data from crushing, and only samples with > 0.19 μcc/g of ^{4}He are included; errors are ± 1σ. Dashed line is a best fit regression: ^{3}He/^{4}He = 0.0714*Longitude + 5.54. Total distance between dredges is 490 km; average dredge spacing is 23 km.

Fig. 5. ^{3}He/^{4}He variations for basalt glass dredged along the Southern Mid-Atlantic Ridge between 1°-47°S (data from Staudacher et al., 1989; Graham et al., 1992, 1996; Kurz et al., 1998; Sarda et al., 2000; Moreira et al, 1995; Stroncik et al., 2007). Three samples with ^{4}He < 0.02 μcc/g are not plotted). Unpublished data from MAR 31.4°-34.1°S was provided by Dave Graham (Hanan, Graham and Michael, 1994). The only major ^{3}He/^{4}He anomalies are associated with the Discovery (D) and Shona (S) hotspots, 48°-52°S. The open symbols in the top panel are data from off-axis seamounts along the Moore Fracture zone (Graham et al., 1996), and near 10°S (Stroncik et al., 2007). Locations of other off-axis island hotspots (projected onto the ridge) are indicated along the top of the upper panel: Ascension (A), St. Helena (SH), Tristan (T) and Gough (G).The lower panel is an enlargement of the best sampled segment between 25.7°S and 26.5°S (Graham et al., 1996), with the bounding fracture zones indicated, along with the location of the topographic axial swell, and the inactive Midway Fracture zone (MDZ). For regional context, arrows A and B indicate the ^{3}He/^{4}He averaged over 650 km north (6 samples, 7.67 Ra) and 650 km south of this segment (8 samples, 7.73 Ra) respectively.

Fig. 6. ^{3}He/^{4}He variations for basalt glass from dredges along the Southern East Pacific Rise, between 13°-29°S (data from Poreda et al., 1993; Niedermann et al., 1997; Kurz et al., 2005). Two large-scale helium isotope anomalies are present in this area, one centered on 17°S (the MELT experiment region), and one running south of 25°S, associated with the Easter microplate and hotspot (the open symbols in the top panel indicate the west rift of the microplate). The lower panel is an enlargement of the relatively "normal" region between these two anomalies. The dashed line labeled "OSC" is the location of the overlapping spreading center at 20.7°S that delineates a sharp Sr, Nd and Pb isotopic boundary (Mahoney et al., 1994), but with no associated ^{3}He/^{4}He variation.
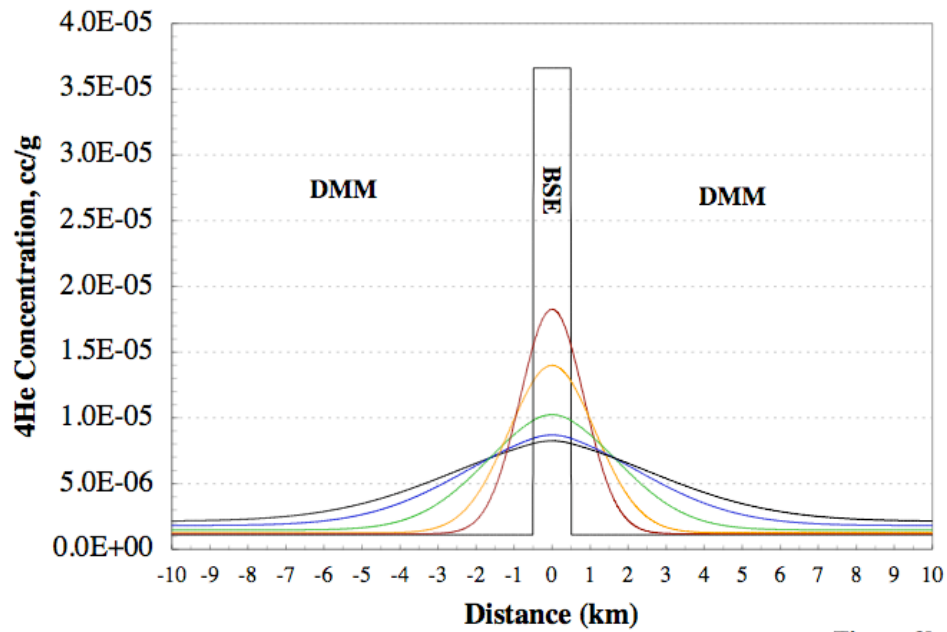
Figure 1

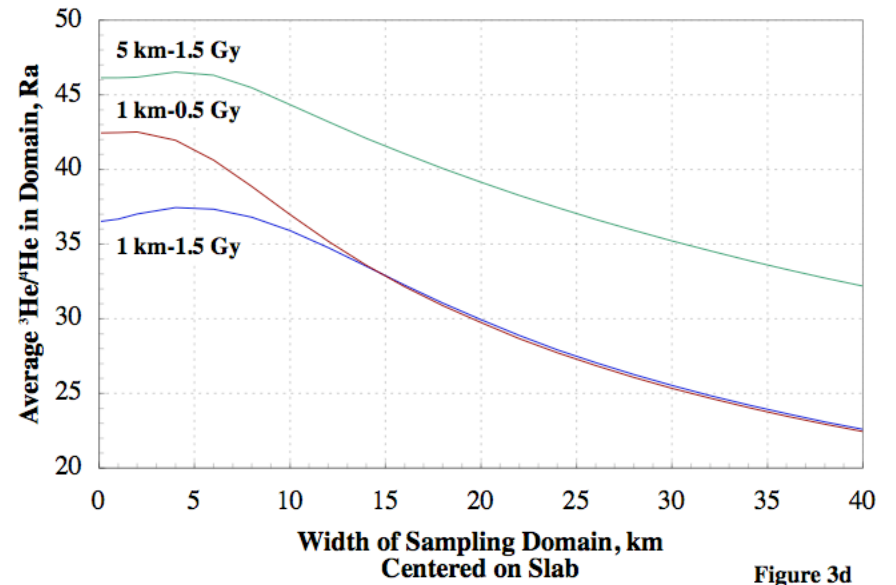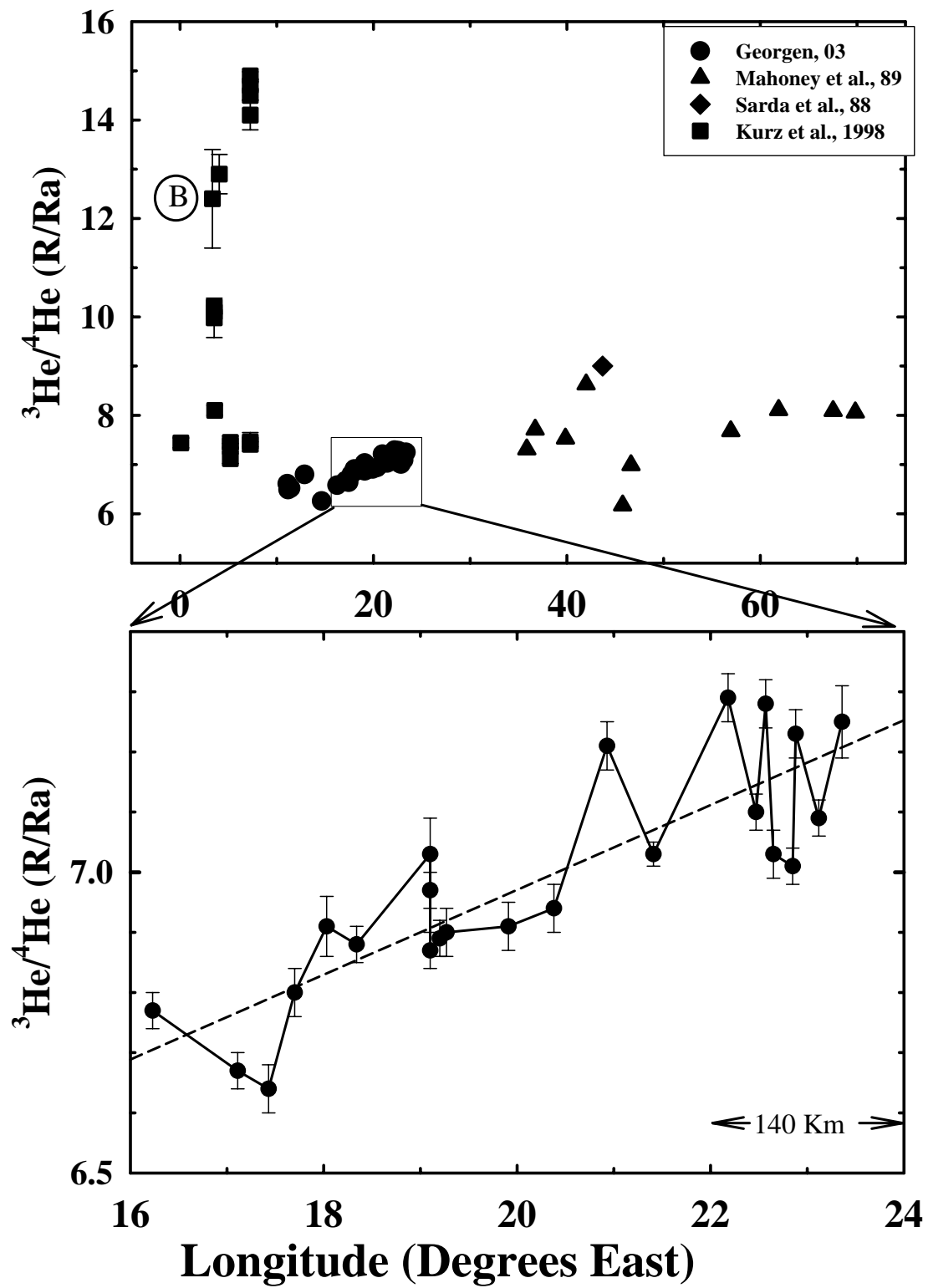Figure 2a

Figure 2c
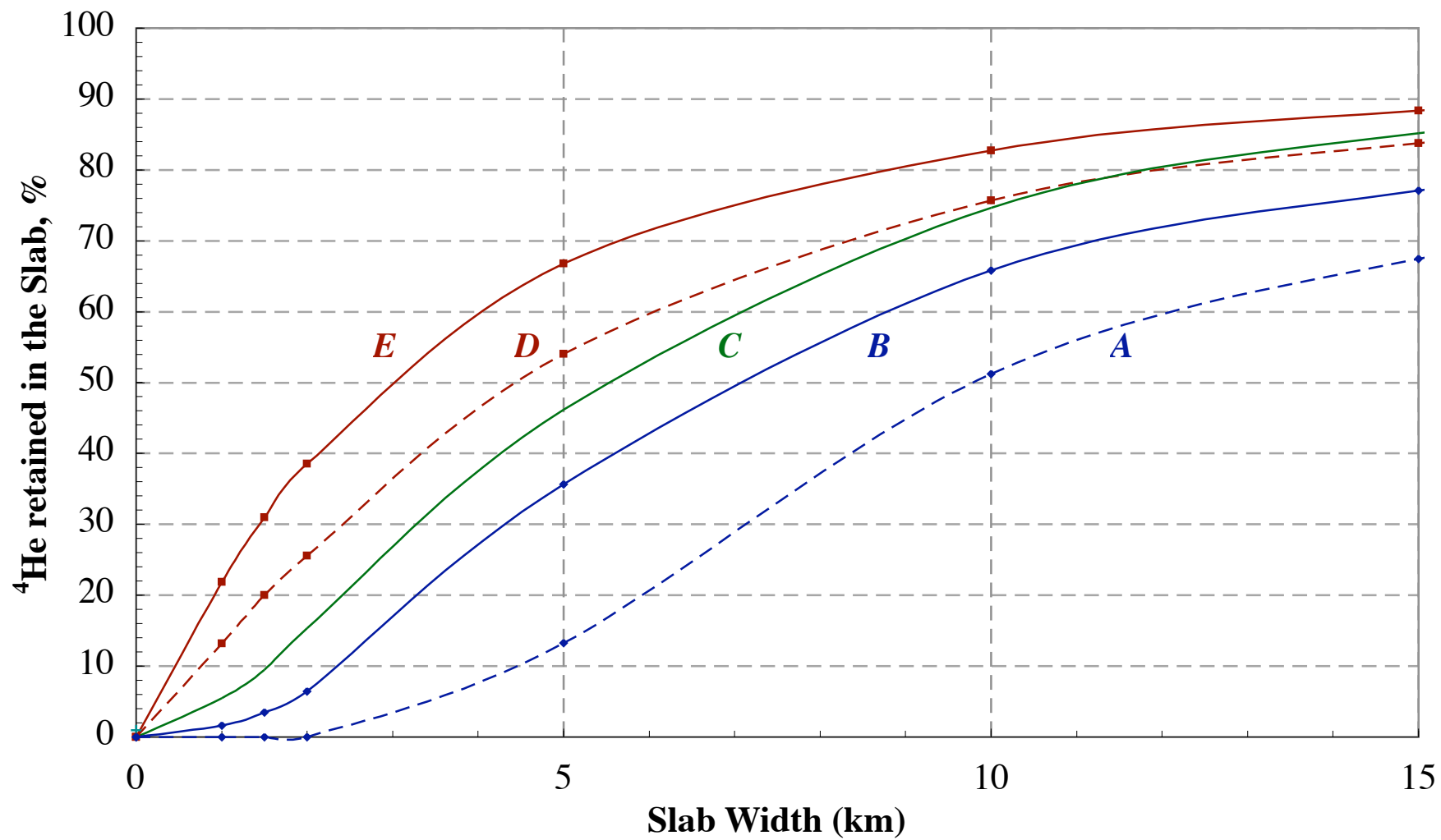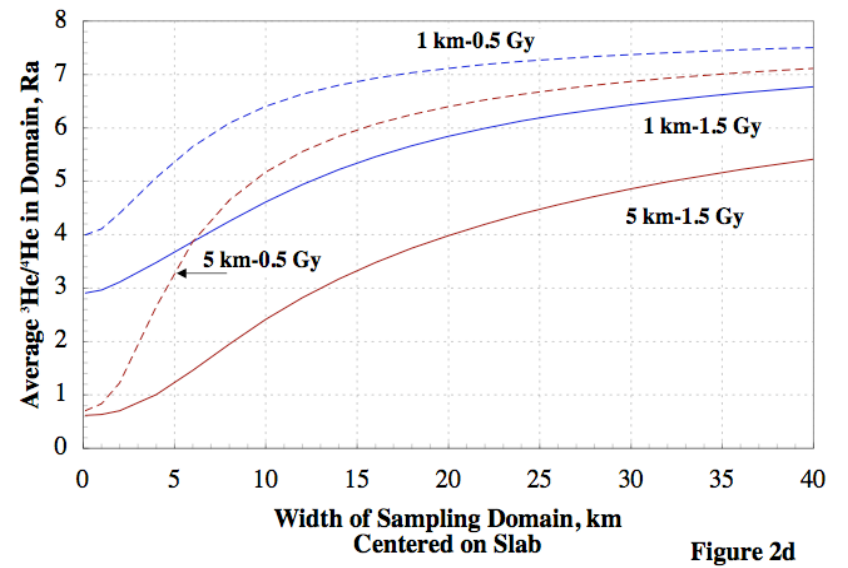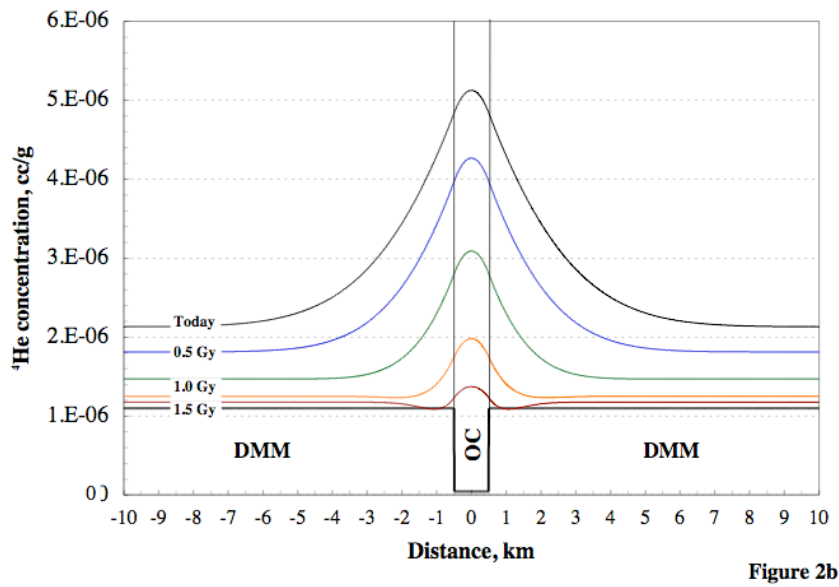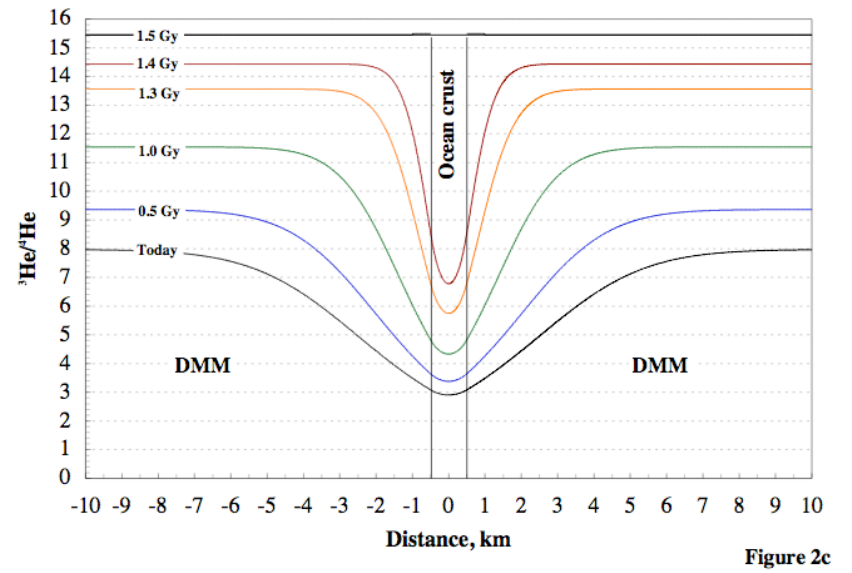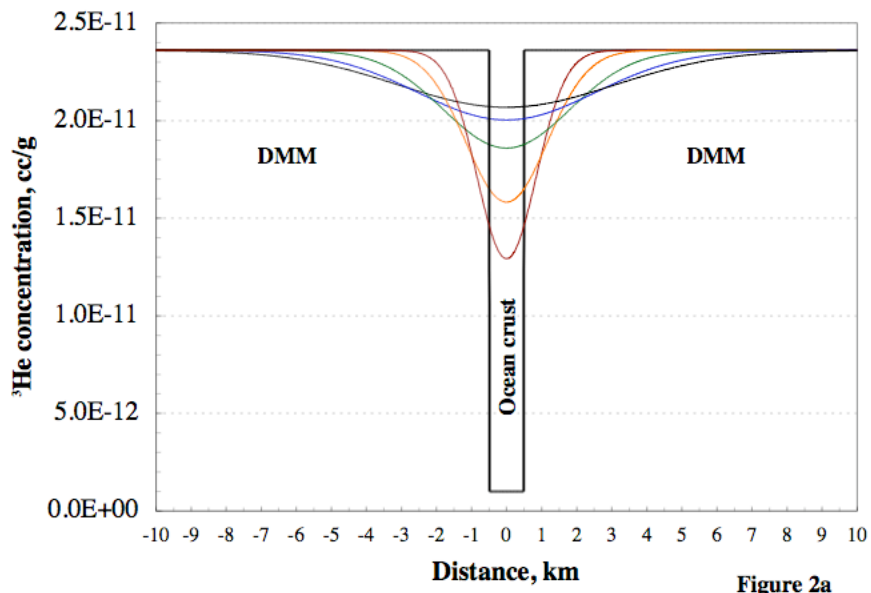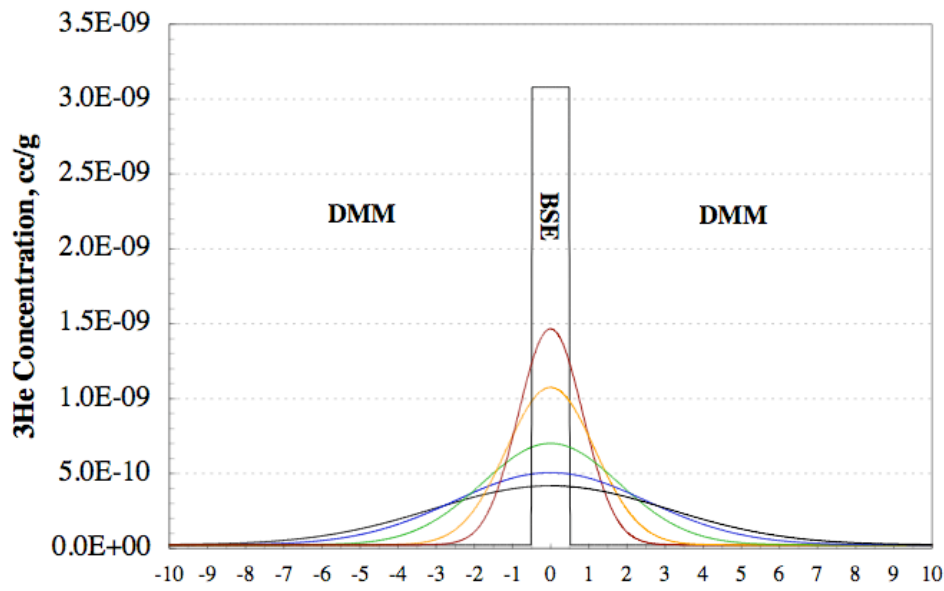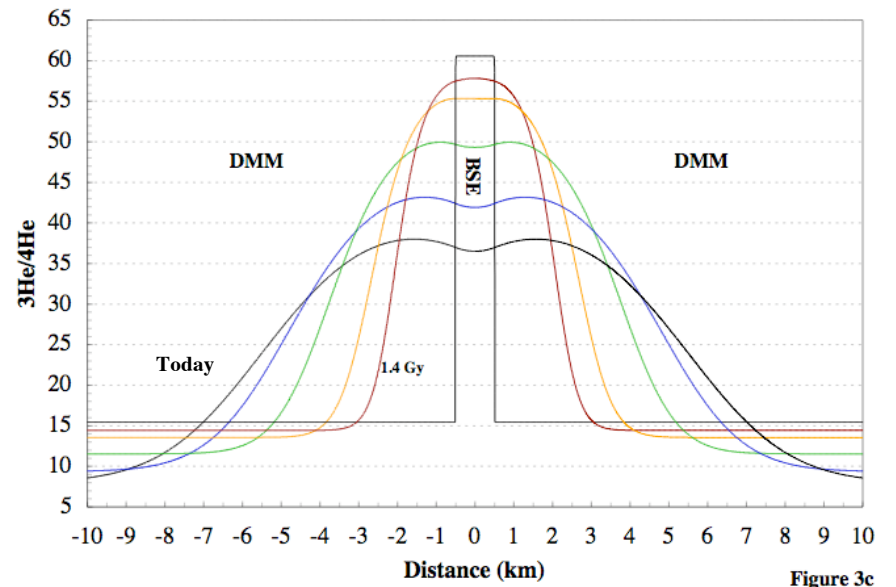
Figure 2b

Figure 2d

Figure 3b

Figure 3c

Figure 3d

Figure 4
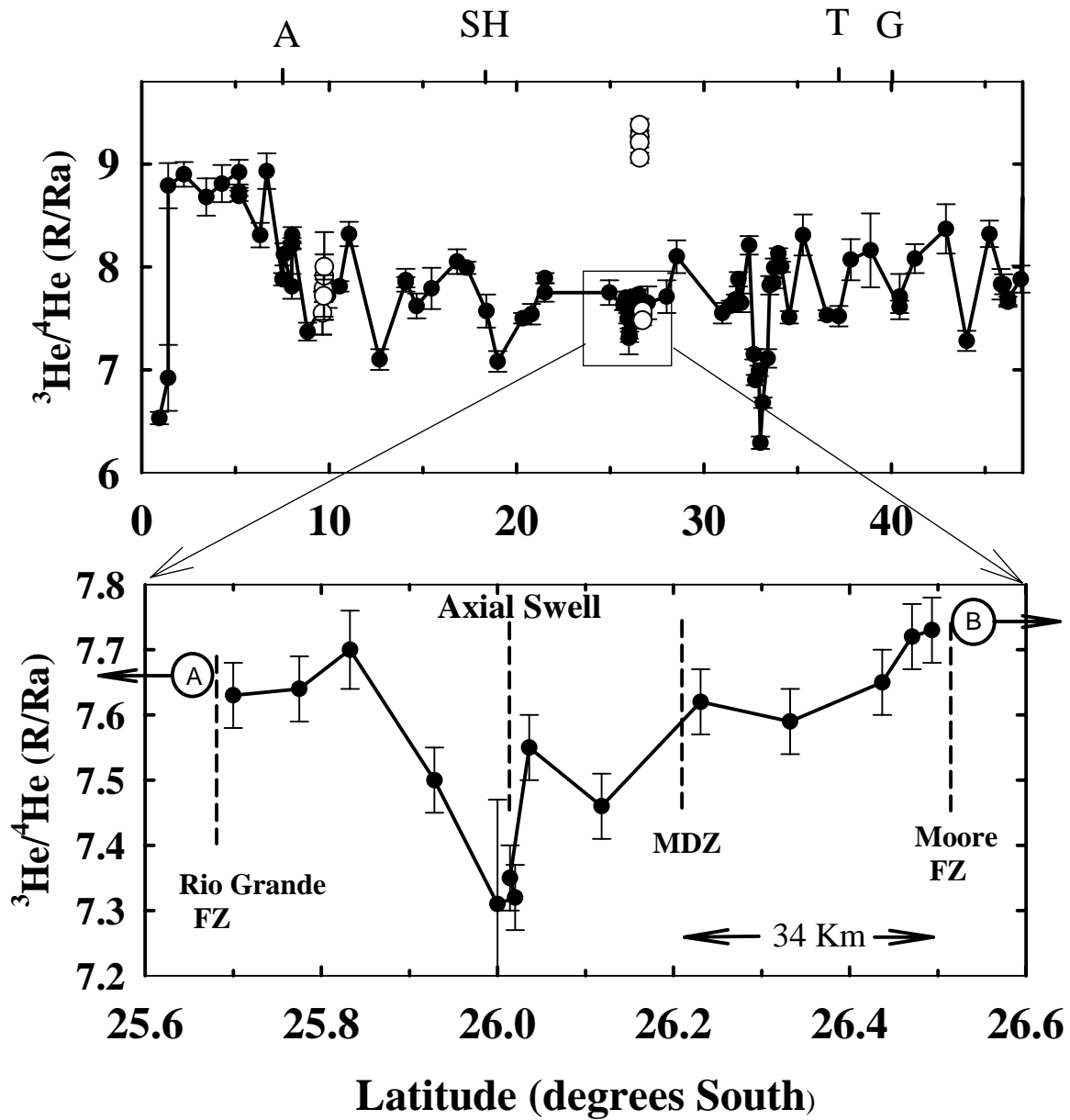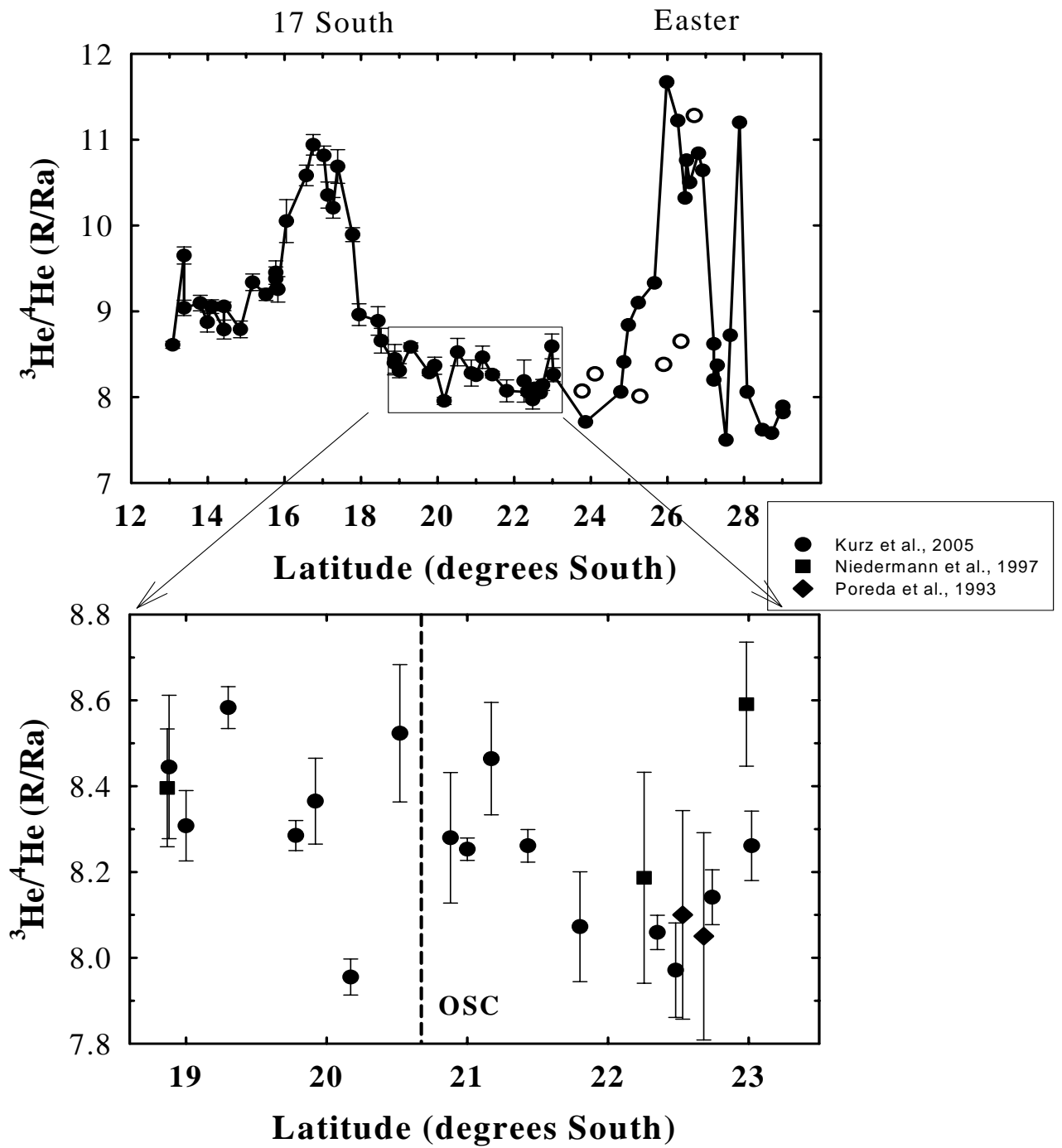
Figure 5

Figure 6

Table 1 - U - Th - He Input Parameters for Slab Models

Reservoir	BSE	DMM	Ocean Crust	BSE	DMM	Ocean Crust
Age, Gy	1.5	1.5	1.5	today	today	today
U, ppb				20.0	3.2	46.0
Th/U				4.0	2.5	2.5
3He, cc/g	3.08E-09	2.36E-11	1.00E-12	3.08E-09	2.36E-11	1.00E-12
4He, cc/g	3.66E-05	1.10E-06	4.65E-08	4.43E-05	2.12E-06	1.48E-05
3/4He	60.57	15.49	15.49	50	8	0.04872
238U/3He (today)				607	12690	4.30E+06

For discussion of data selection, see Appendix II. Footnotes to Table 1